Journal of Materials Chemistry A

COMMUNICATION

Direct electrodeposition of cobalt oxide nanosheets on carbon paper as free-standing cathode for Li–O_2 battery†

Cite this: *J. Mater. Chem. A*, 2014, **2**, 6081

Received 6th October 2013
Accepted 8th November 2013

DOI: 10.1039/c3ta14011c

www.rsc.org/MaterialsA

Qing-chao Liu,‡[ac] Ji-jing Xu,‡[a] Zhi-wen Chang[ab] and Xin-bo Zhang*[a]

Cobalt oxide nanosheets (Co_3O_4 NSs) are grown on carbon paper (CP) by an efficient and facile electrodeposition method. When directly used as free-standing cathode for lithium–oxygen batteries, the Co_3O_4 NSs/CP is found to be robust and shows enhanced specific capacity and cycling stability.

Rechargeable lithium–air (O_2) batteries are receiving great interest thanks to their very high theoretical energy density, far exceeding that of lithium-ion batteries.[1–4] However, to make it a reality, many scientific and technological challenges should be addressed, including (i) the instability of the electrolyte in the cell environment,[5–8] (ii) the decomposition of carbon above 3 V (attacked by intermediates of Li_2O_2, which actively promotes electrolyte decomposition on discharge and charge),[9] (iii) the precipitation of insoluble discharge product, Li_2O_2, blocking the void of the O_2 cathode and eventually limiting the battery performance,[10–13] and (iv) the insufficient structural stability of the cathode caused by reaction products on cycling.[14] All these seriously lead to capacity fading on cycling and premature cell death. Up to now, intensive research effort has been devoted to overcome these limitations by reducing overpotentials to alleviate electrolyte decomposition,[15] tuning the porous structure to provide sufficient 'highways' and 'sites' for improving cycle stability,[16–18] and tailoring the cathode structure to enhance structural stability. Although significant progress has been achieved, development of an effective cathode to further improve the performance of Li–O_2 batteries is still needed.

Carbon supported catalysts have been widely used in cathodes for Li–O_2 batteries due to their enhanced electronic conductivity and catalytic activity.[19–24] However, the carbon itself and the commonly used organic binder (*e.g.* PVDF) are reported to be unstable in Li–O_2 batteries.[25] To solve these problems, development of a free-standing (binder-free) and/or non-carbon dominant cathode is proposed recently.[26–31] Herein, we report an efficient and facile electrodeposition method to fabricate a free-standing cathode with Co_3O_4 nanosheets arrays vertically grown from carbon paper (Co_3O_4 NSs/CP) without any polymer binder, which endows the Li–O_2 battery with enhanced specific capacity of 2159 mA h g^{-1} (based on weight of Co_3O_4) and cycling performance. The structure of the rechargeable Li–O_2 battery based on Co_3O_4 NSs/CP free-standing cathode is schematically illustrated in Scheme 1.

The morphology and structure of the Co_3O_4 NSs/CP are investigated by scanning electron microscopy (SEM) and transmission electron microscopy (TEM). From the low-magnification SEM image (Fig. 1a) of Co_3O_4 NSs/CP, the Co_3O_4 NSs are uniformly vertically grown on the CP skeletons, which ensures the formation of a free-standing structure and a

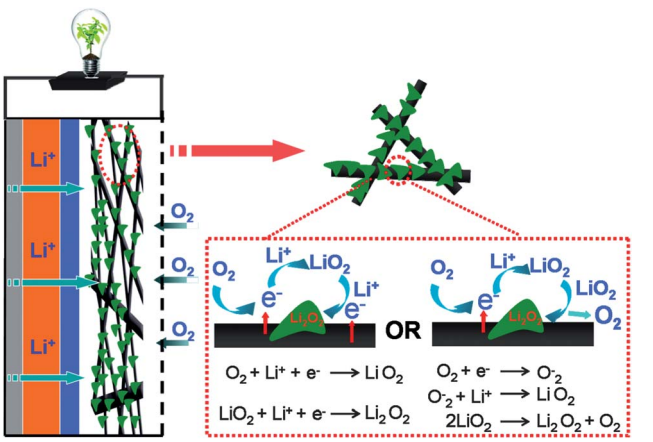

Scheme 1 Schematic of the proposed Co_3O_4 NSs/CP based Li–O_2 cell.

[a]*State Key Laboratory of Rare Earth Resource Utilization, Changchun Institute of Applied Chemistry, Chinese Academy of Sciences, Changchun, 130022, China. E-mail: xbzhang@ciac.ac.cn; Fax: +86-431-85262235; Tel: +86-431-85262235*

[b]*Graduate University of Chinese Academy of Sciences, Beijing, 100049, China*

[c]*School of Materials Science and Engineering, Jilin University, Changchun, 130012, China*

† Electronic supplementary information (ESI) available. See DOI: 10.1039/c3ta14011c

‡ These authors contributed equally to this work.

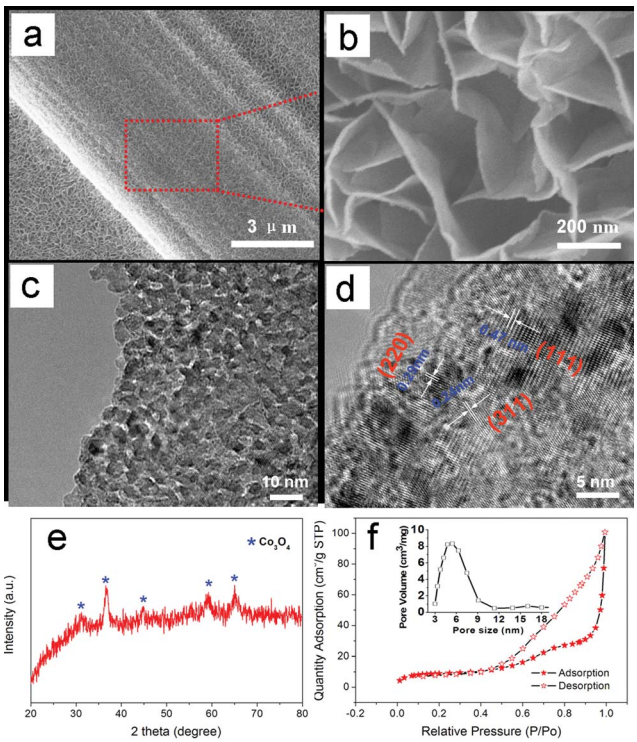

Fig. 1 SEM images of the Co_3O_4 NSs/CP at (a) low-magnification and (b) high-magnification. (c) TEM image, (d) HRTEM image and (e) XRD pattern. (f) Nitrogen adsorption–desorption isotherm and pore-size distribution curves (inset).

favorable low-resistance pathway for electron transfer (free of binder). High-magnification observation reveals that the Co_3O_4 sheets have a thickness of *ca.* 6 nm and are interconnected with each other, forming a highly open and porous structure (Fig. 1b), which ensures that the Co_3O_4 NSs surface is highly accessible by electrolyte and O_2. The TEM image of the Co_3O_4 NSs clearly shows that the nanosheets consist of numerous interconnected nanoparticles with a size of about 5 nm forming a mesoporous structure (Fig. 1c). A high-resolution TEM (HRTEM) image (Fig. 1d) collected at the surface of the Co_3O_4 NSs reveals the lattice fringes of 0.29 nm in (220) planes, 0.47 nm in (111) planes, and 0.24 nm in (311) planes, corresponding to spinel Co_3O_4, which is further confirmed by X-ray diffraction (XRD) (space group: *Fd3m* (227), JCPDS no. 42-1467) (Fig. 1e). The N_2-adsorption isotherm and the pore-size distribution are shown in Fig. 1f. It can be found that the Co_3O_4 NSs exhibit a specific surface area of 28.77 $m^2\ g^{-1}$. The pore-size-distribution data shows that the major size of the pores falls into the range of 4–8 nm. When directly used as the O_2 cathode, the thus obtained Co_3O_4 NSs/CP could essentially hold many tailored properties for Li–O_2 battery: (1) the direct contact of Co_3O_4 NSs with high-conductive CP without binder could facilitate the continuous and high flux of electron transfer throughout the cathode; (2) the open macropores between the Co_3O_4 NSs offer sufficient channels to transfer O_2, electrolyte, and reaction intermediate species freely to/from the inner cathode, ensuring uniform reactant distributions; (3) the mesoporous nature provided by Co_3O_4 NSs offers abundant catalytic sites for the oxygen reduction (ORR) and oxygen evolution reactions (OER); (4) this bimodal design of hierarchically porous structure and the interconnected Co_3O_4 NSs sustain structural stability of cathode and long cycle performance. All of these advantages would benefit the electrochemical performance of the Li–O_2 battery.

The electrochemical performance of Li–O_2 cells with Co_3O_4 NSs/CP cathode are displayed in Fig. 2. Tetraethylene glycol dimethyl ether containing $LiCF_3SO_3$ is selected as electrolyte because of its relatively high stability toward O_2^-.[32–34] The first galvanostatic charge–discharge profiles are shown in Fig. 2a. The cell with the Co_3O_4 NSs/CP cathode exhibits a higher discharge capacity of 2159 mA h g^{-1} than that of Co_3O_4 NSs pasted on CP with PVDF (330.5 mA h g^{-1}) at a current density of 100 mA g^{-1}, indicating that the Co_3O_4 NSs/CP cathode provides more void space for discharge product deposition. The capacity of Li–O_2 cell with pristine CP cathode is 240 mA h g^{-1}, which is almost one-tenth that of the cell with Co_3O_4 NSs/CP cathode. Furthermore, to exclude the possible electrochemical contributions from intercalation reactions with CP and/or Co_3O_4 NSs, the cathode is also discharged in pure argon with the same current density. Clearly, the capacity is negligible (5.2 mA h g^{-1}), suggesting that the oxygen-containing reaction dominates the discharge capacities of the Li–O_2 cells with Co_3O_4 NSs. The cell with Co_3O_4 NSs/CP cathode is then recharged up to 4.4 V and around 2265 mA h g^{-1} is obtained, which is similar to the discharge capacity and shows the relatively high rechargeability of Li–O_2 cells with Co_3O_4 NSs, which is further supported by the electrochemical impedance spectra (EIS). As shown in Fig. 2b, it is found that after the first discharge, the impedances of the cell increase significantly, which is due to the very poor electronic conductive of discharge products generated in the cathode. Interestingly, after recharging, the impedance of the cell almost gets back to the initial value, indicating that the insulated discharge products can be nearly fully decomposed during charge, which is consistent with the SEM images of Fig. 3b, highlighting again the relatively high rechargeability of the Li–O_2 cells with Co_3O_4 NSs/CP cathode.

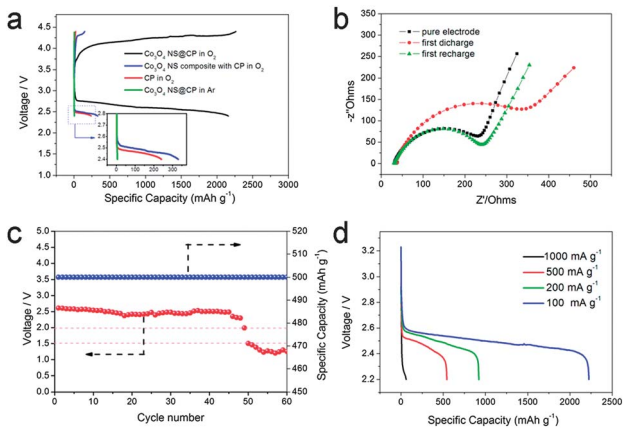

Fig. 2 (a) First charge–discharge profiles, (b) electrochemical impedance spectra, (c) cycling performance, and (d) the rate performance of Li–O_2 cell with Co_3O_4 NSs/CP cathode.

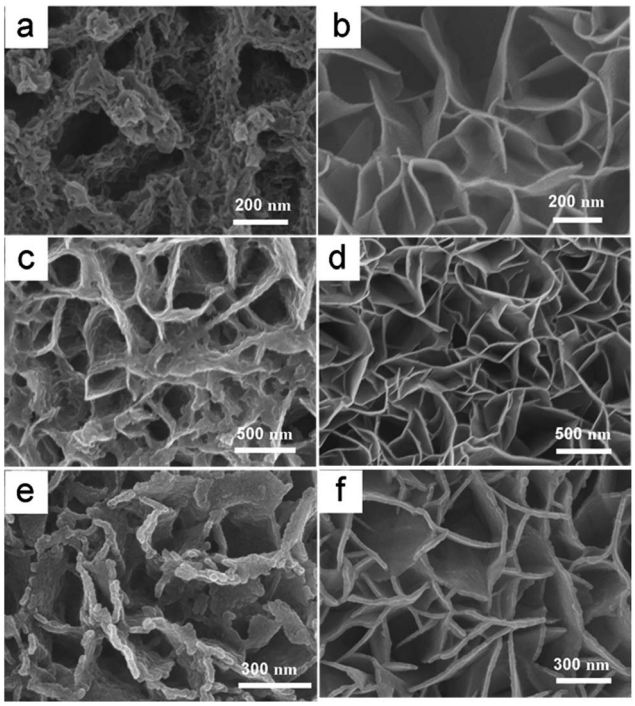

Fig. 3 SEM images of the Co_3O_4 NSs/CP cathode (a) discharged and (b) charged after one cycle, (c) discharged and (d) charged after 20 cycles and, (e) discharged and (f) charged after 40 cycles with the capacity limited to 500 mA h g^{-1}.

Following the recently widely used capacity-limited cycle method, Fig. 2c displays the cycle performance of the Li–O_2 cell with Co_3O_4 NSs/CP cathode at a current density of 100 mA g^{-1} with the capacity limited to 500 mA h g^{-1}. After 49 cycles, the cut-off voltage is still above 2.0 V. The battery is then tested with the capacity limited to 800 mA h g^{-1}, as shown in Fig. S2,† 25 stable cycles are obtained, further showing the enhanced stability of Li–O_2 cells with the Co_3O_4 NSs/CP cathode. One possible factor of this enhanced cycling performance is the cathode structure – the macropores between Co_3O_4 NSs grown on the cathode provide ample space for discharge product formation and decomposition. Another possible reason is the unique nanosheet-shape structure of the generated Li_2O_2 (Fig. 3a), which ensures a uniform electrolyte distribution around the discharge products and promotes the decomposition of the product during charge. And finally, the mechanical stability of the cathode might also contribute to the enhanced cycling performance. Fig. 2d shows the discharge curves of Li–O_2 cells with the Co_3O_4 NSs/CP cathode at different current densities. Interestingly, the discharge capacity at the current density of 500 mA g^{-1} can still reach 542 mA h g^{-1}. For comparison, the cycling performance and rate capability of Li–O_2 cell based on CP and Co_3O_4 NSs-CP cathode are illustrated in Fig. S3 and S4,† respectively.

Fig. 3 shows the morphology variation of the Co_3O_4 NSs/CP cathode at different discharge–charge cycle stages with capacity limited to 500 mA h g^{-1} (Fig. 3). Unlike toroidal morphology that has been widely reported by many other groups,[35–40] the discharge products formed on the Co_3O_4 NSs/CP cathode after the first cycle are nanosheets which uniformly grow vertically onto Co_3O_4 NSs (Fig. 3a). The uniformly and loosely distributed nanosheets could provide sufficient product–electrolyte interfaces, which promote subsequent charge processes and finally enhance the performance of Li–O_2 cell. The SEM images also show the rechargeability of the cathode (Fig. 3b). It can be found that clean Co_3O_4 NSs can be almost recovered in the following recharged stage, which is consistent with the above EIS results (Fig. 2b). In order to further confirm the stability of the Co_3O_4 NSs/CP cathode in a Li–O_2 cell upon cycling, the morphology changes of the recharged O_2 cathodes after the 20th and 40th cycle are examined. It is found that, even after the 40th charge, the Co_3O_4 NSs can still be recovered. This result further confirms the superiority of the Co_3O_4 NSs/CP cathode in terms of rechargeability and stability. The morphology changes of the Co_3O_4 NSs/CP cathode used in Li–O_2 cells with capacity limited to 800 mA h g^{-1} at different discharge–charge cycle stages are shown in Fig. S5,† which also demonstrate rechargeability and stability of the Co_3O_4 NSs/CP cathode. For comparison, the morphology evolution of the CP cathode and Co_3O_4 NSs pasted on CP composite cathode are shown in Fig. S6,† wherein only toroidal Li_2O_2 can be obtained. Besides, there is still some Li_2O_2 on those two cathodes after recharging, which indicates the poor rechargeability of those two cathodes.

Investigation of the formation and decomposition processes of discharge products is crucial for the understanding of the electrochemical behavior in the Li–O_2 battery. The XRD pattern shows that the peak of Li_2O_2 is very weak, indicating the poor crystallinity of Li_2O_2 (Fig. S7†). Alternatively, Fourier transform infrared (FTIR) spectroscopy is then employed to investigate the discharge products. As shown in Fig. 4a, though a small quantity of Li_2CO_3 is formed after the first discharge, the dominant product is found to be Li_2O_2. It should be noted that the discharge product can be almost decomposed during the following recharge process, which is in agreement with the above obtained EIS (Fig. 2b) and SEM results (Fig. 3b). Furthermore, the galvanostatic intermittent titration technique (GITT) measurement[41,42] shows that the equilibrium potential of the Li–O_2 battery is near 2.9 V regardless of the state of charge, which is in accordance with the formation potential of Li_2O_2.[43–45]

In summary, a robust free-standing Co_3O_4 NSs/CP cathode is fabricated by a facile and efficient electrodeposition method. When directly employed as O_2 cathode, the Li–O_2 battery shows

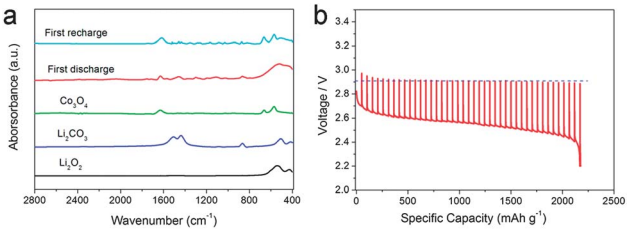

Fig. 4 (a) FTIR spectra of the Co_3O_4 NSs/CP cathode at the first discharge and recharge stage. The reference spectra for Li_2O_2, Li_2CO_3 and Co_3O_4 are also shown for comparison. (b) GITT discharge voltage profile obtained from the Li–O_2 cell with Co_3O_4 NSs/CP cathode.

a high capacity and enhanced cycling capability, which might be attributed to the catalytic activity, bimodal pore structure, and robust structure of the Co_3O_4 NSs/CP cathode. Although the presence of side reactions as well as the low electrical conductivity of transition metal oxide catalysts might limit their application in Li–O_2 batteries, these problems might be solved by element doping and engineering the reaction interface,[46,47] which needs to be further investigated.

Acknowledgements

This work was financially supported by 100 Talents Programme of The Chinese Academy of Sciences, National Program on Key Basic Research Project of China (973 Program, Grant no. 2012CB215500), Foundation for Innovative Research Groups of the National Natural Science Foundation of China (Grant no. 20921002) and National Natural Science Foundation of China (Grant no. 21101147).

References

1 Y. Wang, P. He and H. Zhou, *Energy Environ. Sci.*, 2011, **4**, 4994–4999.
2 K. M. Abraham and Z. Jiang, *J. Electrochem. Soc.*, 1996, **143**, 1–5.
3 Y.-C. Lu, H. A. Gasteiger, M. C. Parent, V. Chiloyan and Y. Shao-Horn, *Electrochem. Solid-State Lett.*, 2010, **13**, A69–A72.
4 J. P. Zheng, R. Y. Liang, M. Hendrickson and E. J. Plichta, *J. Electrochem. Soc.*, 2008, **155**, A432–A437.
5 M. Leskes, N. E. Drewett, L. J. Hardwick, P. G. Bruce, G. R. Goward and C. P. Grey, *Angew. Chem., Int. Ed.*, 2012, **51**, 8560–8563.
6 S. A. Freunberger, Y. Chen, Z. Peng, J. M. Griffin, L. J. Hardwick, F. Bardé, P. Novák and P. G. Bruce, *J. Am. Chem. Soc.*, 2011, **133**, 8040–8047.
7 D. Xu, Z.-l. Wang, J.-j. Xu, L.-l. Zhang, L.-m. Wang and X.-b. Zhang, *Chem. Commun.*, 2012, **48**, 11674–11676.
8 W. Walker, V. Giordani, J. Uddin, V. S. Bryantsev, G. V. Chase and D. Addison, *J. Am. Chem. Soc.*, 2013, **135**, 2076–2079.
9 M. M. Ottakam Thotiyl, S. A. Freunberger, Z. Peng and P. G. Bruce, *J. Am. Chem. Soc.*, 2013, **135**, 494–500.
10 J. Hou, M. Yang, M. W. Ellis, R. B. Moore and B. Yi, *Phys. Chem. Chem. Phys.*, 2012, **14**, 13487–13501.
11 R. R. Mitchell, B. M. Gallant, C. V. Thompson and Y. Shao-Horn, *Energy Environ. Sci.*, 2011, **4**, 2952–2958.
12 V. Viswanathan, K. S. Thygesen, J. S. Hummelshøj, J. K. Nørskov, G. Girishkumar, B. D. McCloskey and A. C. Luntz, *J. Chem. Phys.*, 2011, **135**, 214704.
13 L. Zhong, R. R. Mitchell, Y. Liu, B. M. Gallant, C. V. Thompson, J. Y. Huang, S. X. Mao and Y. Shao-Horn, *Nano Lett.*, 2013, **13**, 2209–2214.
14 B. M. Gallant, R. R. Mitchell, D. G. Kwabi, J. Zhou, L. Zuin, C. V. Thompson and Y. Shao-Horn, *J. Phys. Chem. C*, 2012, **116**, 20800–20805.
15 J.-L. Shui, N. K. Karan, M. Balasubramanian, S.-Y. Li and D.-J. Liu, *J. Am. Chem. Soc.*, 2012, **134**, 16654–16661.
16 J. Nanda, H. Bilheux, S. Voisin, G. M. Veith, R. Archibald, L. Walker, S. Allu, N. J. Dudney and S. Pannala, *J. Phys. Chem. C*, 2012, **116**, 8401–8408.
17 H.-D. Lim, K.-Y. Park, H. Song, E. Y. Jang, H. Gwon, J. Kim, Y. H. Kim, M. D. Lima, R. O. Robles, X. Lepró, R. H. Baughman and K. Kang, *Adv. Mater.*, 2013, **25**, 1348–1352.
18 J. Xiao, D. Mei, X. Li, W. Xu, D. Wang, G. L. Graff, W. D. Bennett, Z. Nie, L. V. Saraf, I. A. Aksay, J. Liu and J.-G. Zhang, *Nano Lett.*, 2011, **11**, 5071–5078.
19 J.-J. Xu, D. Xu, Z.-L. Wang, H.-G. Wang, L.-L. Zhang and X.-B. Zhang, *Angew. Chem., Int. Ed.*, 2013, **52**, 3887–3890.
20 L. Zhang, X. Zhang, Z. Wang, J. Xu, D. Xu and L. Wang, *Chem. Commun.*, 2012, **48**, 7598–7600.
21 H. Cheng and K. Scott, *J. Power Sources*, 2010, **195**, 1370–1374.
22 N. Ominde, N. Bartlett, X.-Q. Yang and D. Qu, *J. Power Sources*, 2010, **195**, 3984–3989.
23 R. Black, J.-H. Lee, B. Adams, C. A. Mims and L. F. Nazar, *Angew. Chem., Int. Ed.*, 2013, **52**, 392–396.
24 S. H. Oh, R. Black, E. Pomerantseva, J. H. Lee and L. F. Nazar, *Nat. Chem.*, 2012, **4**, 1004–1010.
25 R. Black, S. H. Oh, J.-H. Lee, T. Yim, B. Adams and L. F. Nazar, *J. Am. Chem. Soc.*, 2012, **134**, 2902–2905.
26 A. Riaz, K.-N. Jung, W. Chang, S.-B. Lee, T.-H. Lim, S.-J. Park, R.-H. Song, S. Yoon, K.-H. Shin and J.-W. Lee, *Chem. Commun.*, 2013, **49**, 5984–5986.
27 Y. Cui, Z. Wen and Y. Liu, *Energy Environ. Sci.*, 2011, **4**, 4727–4734.
28 Z. Peng, S. A. Freunberger, Y. Chen and P. G. Bruce, *Science*, 2012, **337**, 563–566.
29 G. Q. Zhang, J. P. Zheng, R. Liang, C. Zhang, B. Wang, M. Hendrickson and E. J. Plichta, *J. Electrochem. Soc.*, 2010, **157**, A953–A956.
30 R. R. Mitchell, B. M. Gallant, C. V. Thompson and Y. Shao-Horn, *Energy Environ. Sci.*, 2011, **4**, 2952–2958.
31 Z.-L. Wang, D. Xu, J.-J. Xu, L.-L. Zhang and X.-B. Zhang, *Adv. Funct. Mater.*, 2012, **22**, 3699–3705.
32 H.-G. Jung, J. Hassoun, J.-B. Park, Y.-K. Sun and B. Scrosati, *Nat. Chem.*, 2012, **4**, 579–585.
33 S. A. Freunberger, Y. Chen, N. E. Drewett, L. J. Hardwick, F. Bardé and P. G. Bruce, *Angew. Chem., Int. Ed.*, 2011, **50**, 8609–8613.
34 Y. Chen, S. A. Freunberger, Z. Peng, F. Bardé and P. G. Bruce, *J. Am. Chem. Soc.*, 2012, **134**, 7952–7957.
35 B. D. Adams, C. Radtke, R. Black, M. L. Trudeau, K. Zaghib and L. F. Nazar, *Energy Environ. Sci.*, 2013, **6**, 1772–1778.
36 B. M. Gallant, D. G. Kwabi, R. R. Mitchell, J. Zhou, C. V. Thompson and Y. Shao-Horn, *Energy Environ. Sci.*, 2013, **6**, 2518–2528.
37 R. R. Mitchell, B. M. Gallant, Y. Shao-Horn and C. V. Thompson, *J. Phys. Chem.*, 2013, **4**, 1060–1064.

38 E. Yilmaz, C. Yogi, K. Yamanaka, T. Ohta and H. R. Byon, *Nano Lett.*, 2013, **13**, 4679–4684.
39 J. Lu, Y. Lei, K. C. Lau, X. Luo, P. Du, J. Wen, R. S. Assary, U. Das, D. J. Miller, J. W. Elam, H. M. Albishri, D. A. El-Hady, Y.-K. Sun, L. A. Curtiss and K. Amine, *Nat. Commun.*, 2013, **4**, 2383.
40 J.-J. Xu, Z.-L. Wang, D. Xu, L.-L. Zhang and X.-B. Zhang, *Nat. Commun.*, 2013, **4**, 2438.
41 T. Sasaki, Y. Ukyo and P. Novák, *Nat. Mater.*, 2013, **12**, 569–575.
42 W. Weppner and R. A. Huggin, *J. Electrochem. Soc.*, 1977, **124**, 1569–1578.
43 Y.-C. Lu, D. G. Kwabi, K. P. C. Yao, J. R. Harding, J. Zhou, L. Zuin and Y. Shao-Horn, *Energy Environ. Sci.*, 2011, **4**, 2999–3007.
44 H.-K. Lim, H.-D. Lim, K.-Y. Park, D.-H. Seo, H. Gwon, J. Hong, W. A. Goddard, H. Kim and K. Kang, *J. Am. Chem. Soc.*, 2013, **135**, 9733–9742.
45 P. G. Bruce, S. A. Freunberger, L. J. Hardwick and J.-M. Tarascon, *Nat. Mater.*, 2011, **11**, 19–29.
46 X. Lu, M. Yu, G. Wang, T. Zhai, S. Xie, Y. Ling, Y. Tong and Y. Li, *Adv. Mater.*, 2013, **25**, 267–272.
47 H. Cheng, Z. G. Lu, J. Q. Deng, C. Y. Chung, K. Zhang and Y. Y. Li, *Nano Res.*, 2010, **3**, 895–901.